



Ensemble estimates of global wetland methane emissions over 2000-2020

Zhen Zhang¹, Benjamin Poulter², Joe R. Melton³, William J. Riley⁴, George H. Allen⁵, David J. Beerling⁶, Philippe Bousquet⁷, Josep G Canadell⁸, Etienne Fluet-Chouinard⁹, Philippe Ciais⁷, Nicola Gedney¹⁰, Peter O. Hopcroft¹¹, Akihiko Ito¹², Robert B. Jackson¹³, Atul K. Jain¹⁴, Katherine Jensen¹⁵, Fortunat Joos¹⁶, Thomas Kleinen¹⁷, Sara Knox^{18,19}, Tingting Li²⁰, Xin Li¹, Xiangyu Liu²¹, Kyle McDonald¹⁵, Gavin McNicol²², Paul A. Miller²³, Jurek Müller¹⁶, Prabir K. Patra^{24,25}, Changhui Peng²⁶, Shushi Peng²⁷, Zhangcai Qin²⁸, Ryan M. Riggs²⁹, Marielle Saunois⁷, Qing Sun¹⁶, Hanqin Tian³⁰, Xiaoming Xu¹⁴, Yuanzhi Yao³¹, Xi Yi²⁷, Wenxin Zhang²², Qing Zhu⁴, Qian Zhu³², Qianlai Zhuang²¹

10 ¹National Tibetan Plateau Data Center (TPDC), State Key Laboratory of Tibetan Plateau Earth System, Environment and Resource (TPESER), Institute of Tibetan Plateau Research, Chinese Academy of Sciences, Beijing, 100101, China

²NASA Goddard Space Flight Center, Earth Sciences Division, Greenbelt, MD, USA

³Climate Research Division, Environment and Climate Change Canada, Victoria, BC, Canada

⁴Climate and Ecosystem Sciences Division, Lawrence Berkeley National Laboratory, Berkeley, California, USA

15 ⁵Department of Geosciences, Virginia Polytechnic Institute and State University, Blacksburg, VA, USA

⁶School of Biosciences, University of Sheffield, U.K.

⁷Laboratoire des Sciences du Climat et de l'Environnement, CEA, CNRS, UVSQ, universit& Paris-Saclay, Gif sur Yvette, France

⁸Global Carbon Project, CSIRO Environment, ACT 2601, Australia

20 ⁹Earth Systems Science Division, Pacific Northwest National Laboratory, Richland, WA 99352, USA

¹⁰Met Office Hadley Centre, Joint Centre for Hydrometeorological Research, Wallingford, U.K.

¹¹School of Geography, Earth & Environmental Sciences, University of Birmingham, U.K.

¹²National Institute for Environmental Studies, Tsukuba, Japan

25 ¹³Department of Earth System Science, Woods Institute for the Environment, and Precourt Institute for Energy, Stanford University, Stanford, CA 94305–2210, USA

¹⁴Department of Atmospheric Sciences, University of Illinois, Urbana, IL 61821, USA

¹⁵Department of Earth and Atmospheric Sciences, City College of New York, City University of New York, NY, USA

¹⁶Climate and Environmental Physics, Physics Institute and Oeschger Centre for Climate Change Research, University of Bern

30 ¹⁷Max Planck Institute for Meteorology, Hamburg, Germany

¹⁸The University of British Columbia, Vancouver, BC, Canada

¹⁹McGill University, Montreal, QC, Canada



- ²⁰LAPC, Institute of Atmospheric Physics, Chinese Academy of Sciences, Beijing, 100029, China
- ²¹Department of Earth, Atmospheric, Planetary Sciences, Purdue University, West Lafayette, IN, USA
- 35 ²²Department of Atmospheric Sciences, University of Illinois, Chicago, IL, USA
- ²³Department of Physical Geography and Ecosystem Science, Lund University, Sölvegatan 12, 223 62, Lund, Sweden
- ²⁴Japan Agency for Marine-Earth Science and Technology (JAMSTEC), Yokohama, Japan
- ²⁵Research Institute for Humanity and Nature (RIHN), Kyoto, Japan
- ²⁶Department of Biology Sciences, University of Quebec at Montreal, C.P. 8888, Succ. Centre-Ville, Montreal, QC H3C
40 3P8, Canada
- ²⁷Sino-French Institute for Earth System Science, Laboratory for Earth Surface Processes, College of Urban and Environmental Sciences, Peking University, Beijing 100871, China
- ²⁸School of Atmospheric Sciences, Sun-Yat-Sen University, and Southern Marine Science and Engineering Guangdong Laboratory (Zhuhai), Zhuhai 519000, China
- 45 ²⁹Department of Geography, Texas A&M University, College Station, TX, USA
- ³⁰Center for Earth System Science and Global Sustainability, Schiller Institute for Integrated Science and Society, Department of Earth and Environmental Sciences, Boston College, Chestnut Hill, MA 02467, USA
- ³¹School of Geographic Sciences, East China Normal University, Shanghai, China
- ³²College of Hydrology and Water Resources, Hohai University, Nanjing, 210098, China
- 50 *Correspondence to:* Zhen Zhang (yuisheng@email.com)

Abstract. Due to ongoing climate change, methane (CH₄) emissions from vegetated wetlands are projected to increase during the 21st century, challenging climate mitigation efforts aimed at limiting global warming. However, despite reports of rising emission trends, a comprehensive evaluation and attribution of recent changes is still lacking. Here we assessed global wetland CH₄ emissions from 2000 to 2020 based on an ensemble of sixteen process-based wetland models. Our results
55 estimated global average wetland CH₄ emissions at 158±24 (mean ± 1σ) Tg CH₄ yr⁻¹ for the period 2010-2020, with an average decadal increase of 6-7 Tg CH₄ yr⁻¹ compared to the decade of 2000-2009. The increases in the four latitudinal bands of 90°S-30°S, 30°S- 30°N, 30°N-60°N, and 60°N-90°N were 0.1-0.2 Tg CH₄ yr⁻¹, 3.6-3.7 Tg CH₄ yr⁻¹, 1.8-2.4 Tg CH₄ yr⁻¹, and 0.6-0.8 Tg CH₄ yr⁻¹, respectively, over the two decades. The modeled CH₄ sensitivities to temperature show
60 reasonable consistency with eddy covariance-based measurements from 34 sites. Rising temperature was the primary driver of the increase, while precipitation and rising atmospheric CO₂ concentrations played secondary roles with high levels of uncertainty. These modeled results suggest climate change is driving increased wetland CH₄ emissions and that direct and sustained measurements are needed to monitor developments.



1 Introduction

Wetlands are the largest single source in the global methane (CH_4) budget, representing ~25-35% (~150-200 Tg CH_4 yr⁻¹) of the total combined natural and anthropogenic sources (Kirschke et al., 2013; Saunio et al., 2016, 2020). Covering 8-10% of the global land surface (Zhang et al., 2021), wetland area is sensitive to climate variations (Zhang et al., 2018; Zhu et al., 2017). Over the last deglaciation, wetlands played an important role in driving the rise of atmospheric CH_4 concentrations (Hopcroft et al., 2017; Nisbet et al., 2023; Kleinen et al., 2023). In recent decades, wetlands have experienced unprecedented and ongoing changes, including continuous thawing of permafrost (Natali et al., 2019; Treat et al., 2018), land-use change (Fluet-Chouinard et al., 2023), a lengthening of the growing season in the Arctic (Arndt et al., 2019), and expansion in tropical areas due to enhanced precipitation (Fleischmann, 2023). Recent evidence from in situ measurements (Rößger et al., 2022), data driven estimates (Yuan et al., 2024; Ying et al., 2024), and satellite observations (Feng et al., 2022) suggests that these ongoing changes could enhance wetland CH_4 emissions and thus affect the trajectory of atmospheric CH_4 concentration. Furthermore, atmospheric $\delta^{13}\text{C}-\text{CH}_4$ records also show a trend toward increased depletion since the late 2000s (Lan et al., 2021; Nisbet et al., 2019), indicating that isotopically light biogenic sources, such as wetlands (Basu et al., 2022; Feng et al., 2022), agricultural, and waste sources (Schaefer et al., 2016; Zhang, et al., 2021) have become dominant contributors to the rise in atmospheric CH_4 . Current estimates of wetland CH_4 emissions (hereafter denoted as $e\text{CH}_4$) in response to climate change are projected to increase by up to 15-30% by 2050 (Koffi et al., 2020; Zhang et al., 2017), accounting for 25-40% of the pledged reduction in anthropogenic emissions (Shindell et al., 2019). These trends and projections suggest that the emerging wetland- CH_4 climate feedback that influences atmospheric CH_4 concentration requires a better understanding of long-term changes in $e\text{CH}_4$.

Directly diagnosing the variations and trends of $e\text{CH}_4$ at large scales is challenging. Site-level measurements, such as those from chamber and eddy covariance techniques, are useful for identifying underlying mechanisms and monitoring CH_4 fluxes at the landscape scale but are difficult to upscale due to large uncertainties in extrapolation and the high spatial heterogeneity of wetland CH_4 fluxes (Chu et al., 2021; Kuhn et al., 2021). Interpreting $e\text{CH}_4$ using satellite observations and inversions of atmospheric concentration data is also subject to uncertainties in anthropogenic sources, other natural sources, atmospheric chemistry, and model errors associated with atmospheric transport (Gatti et al., 2021; Gloor et al., 2021; Palmer et al., 2022; Patra et al., 2011). Global wetland models, integrated within land biosphere models, can serve to bridge our understanding of wetland CH_4 processes and diagnosing wetland CH_4 dynamics at large scales (Melton et al., 2013; Wania et al., 2013). These models provide mechanistic explanations for the causes of changes in $e\text{CH}_4$ dynamics. Furthermore, recent advances in wetland models (Arora et al., 2018; Kaiser et al., 2017; Shu et al., 2020; Grant 2017; Chang et al. 2020) show significant potential for improving our understanding of $e\text{CH}_4$ through the incorporation of complex biogeochemical processes.



95 Current studies have reached various conclusions on the change in eCH₄ over the last decades. Studies based on single
biogeochemical models (Zhang et al., 2018; Zhu et al., 2017) suggest a significant increase in eCH₄ from 2000-2006 to
2007-2017, while atmospheric inversions (Zhang et al., 2021; Yin et al., 2021; Basu et al., 2022; Feng et al., 2022) suggested
even higher rate increases, from 2 Tg CH₄ yr⁻¹ yr⁻¹ to 3 Tg CH₄ yr⁻¹ yr⁻¹ during the post-2010 period. Poulter et al., (2017)
reported no significant change between the 2000-2006 and 2007-2012 periods based on an ensemble of wetland models,
100 while Saunio et al. (2020) show a slight increase (~2 Tg CH₄ yr⁻¹) in average for 2007-2017 compared to the 2000-2006
level using a large set of wetland CH₄ models. However, these models demonstrate considerable differences in estimated
eCH₄, both spatially and temporally (Ma et al., 2021; Parker et al., 2020; Chang et al., 2023), primarily due to the sensitivity
of their estimations to the wetland areal extent, the implemented biogeochemical structures, and parameterizations. The
multi-model ensemble approach is applied to increase the skill, reliability, and consistency of model forecasts, potentially
105 offsetting individual model errors (Schaefer et al., 2012). However, a recent study (Chang et al. 2023) found that down
selecting atmospheric inversion and wetland model CH₄ predictions based on a comparison to eddy covariance data did not
reduce uncertainty in global eCH₄ estimates. Therefore, it has become necessary to thoroughly evaluate the performance of
these models using the most recent generation of wetland models against an increasingly dense network of observations
(Delwiche et al., 2021; Knox et al., 2019) from eddy covariance sites.

110

Here we conducted ensemble simulations of 16 wetland biogeochemical models following a common modeling protocol to
provide monthly integrated global eCH₄ for the period of 2000-2020, as part of the Global Carbon Project's Methane Budget
activity. The inundation dynamics of each model were simulated using a model-specific prognostic hydrological modeling
approach as well as a set of diagnostic satellite-driven simulations. A set of factorial simulations were carried out to isolate
115 the effects of temperature, precipitation, and rising atmospheric CO₂ concentration. The modeled temperature sensitivity was
evaluated against the global eddy covariance database, FLUXNET-CH₄ (Delwiche et al., 2021; Knox et al., 2019), and a
data-driven global wetland CH₄ upscaling dataset UpCH₄ (McNicol et al., 2023) based on FLUXNET-CH₄. In addition, we
examined the changes in eCH₄ for the year 2020, which was characterized as an extremely warm and wet year with the
highest growth rate of atmospheric CH₄ observed over the study period.

120

2 Methods

2.1 Wetland model ensemble

Sixteen wetland models participated in the ensemble simulations (Table S1). Wetland CH₄ models can be generally
described as functions describing the biogeochemical processes that control CH₄ production and oxidation through
125 methanogenesis and methanotrophy, and the biophysical processes that regulate CH₄ transport from the soil to the
atmosphere (Table S1). Methanogenesis in the models is linked to different proxies (e.g., carbon substrate, heterotrophic



respiration, net primary production) with a wide range of model complexity - more sophisticated models include wetland
Plant Functional Types (PFTs) and explicitly simulate the processes of CH₄ production, consumption, and transport, while
the simplified models use generalized empirical equations to simulate net fluxes without explicitly calculating individual
130 components of the CH₄ flux.

Wetlands were defined as naturally vegetated forested and non-forested ecosystems with saturated/inundated areas,
excluding coastal wetlands, cultivated wetlands such as rice paddies, and open water systems such as rivers, lakes, ponds,
and reservoirs. A prognostic wetland inundation scheme and a diagnostic wetland dataset Wetland Area and Dynamics for
135 Methane Modeling (WAD2M v2; Zhang et al., 2021) are applied to identify the wetland areal dynamics. The prognostic
wetland distribution was independently determined by each model's hydrological modules with different prescribed
parameters. Among the participating models, there was a large variation in complexity and in the level of comprehensiveness
with which wetland extent were characterized. The modules for simulating inundation ranged from simplified TOPMODEL
approaches to more sophisticated representations of water-table variation, with the estimated magnitude being influenced by
140 the hydrologic schemes utilized and the sensitivities to precipitation. The prognostic modeled wetland extent showed large
variability in estimated magnitude but was consistent with satellite-based inundation products in predicting different phases
of inundation (Xi et al., 2022; Zhang, et al., 2021). The ensemble means of the modeled wetland extent demonstrated a
reasonable agreement with the satellite-based product Global Surface Water Extent and Dynamics version 2 (GIEMS2;
Prigent et al., 2020), with high correlations for the temperate region and high latitudes (Fig. S1). The diagnostic runs are
145 exclusively used for temperature dependence calculations due to a discontinuity issue in the WAD2Mv2 over a few tropical
hotspots, which affect a subset of wetland models that are particularly sensitive to inundation in the hotspots.

2.2 Modeling protocol and simulation setups

The modeling protocol aimed to provide wetland CH₄ fluxes and quantify the associated uncertainties arising from model
differences, meteorological forcing, and wetland extent dynamics. To quantify meteorological forcing uncertainty, we used
150 two climate inputs, a ground-based monthly climate dataset from the Climatic Research Unit (CRU) (Harris et al., 2014), up
to 2020 and a harmonized daily dataset from the Global Soil Wetness Project-3 GSWP3-W5E5 through the year 2019, which
is a multiple-source-based daily dataset (Cucchi et al., 2020; Dirmeyer et al., 2006) used in the Inter-Sectoral Impact Model
Intercomparison Project 3a (ISIMIP3a). For models that require 6-hourly meteorological forcings, a temporal-interpolation
dataset CRU-JRA was applied based on the Japanese Reanalysis Agency (JRA55), aligned with CRU. The atmospheric CO₂
155 concentration values for 1861-2020 were obtained from the CMIP6 experimental protocol (Meinshausen et al., 2017).
Ancillary data, such as soil texture and CH₄-related parameter sets used model-specific inputs. All the models were run in
'natural vegetation' mode without transient effects of land use and land cover change. Methane oxidation in wetland soils
was implicitly included in the estimate but the upland oxidative sink was not included as it was not part of the net wetland



emissions calculations. Models included the spin-up period to pre-industrial conditions assuming net ecosystem exchange
160 equilibrium before 1860 by recycling fixed CO₂ concentrations (1860 level of 286.42 ppm) and meteorology (1901-1920).

2.3 FLUXNET-CH₄ and machine learning-based upscaling product UpCH₄

FLUXNET-CH₄ is the first global dataset of CH₄ eddy covariance measurements that includes ~ 80 sites globally, including
different wetland types from peatlands (e.g. bog, fen), mineral wetlands (e.g. marsh, swamp), and rice paddies. For this
study, a subset of natural freshwater wetland sites was selected for the analysis. All the eddy covariance measurements used
165 in this study were gap-filled daily total fluxes filled using an Artificial Neural Network (ANN) approach (Knox et al., 2019).
In addition, a data-driven gridded dataset UpCH₄ (McNicol et al., 2023) for 2001-2018, which is based on 119 site-years of
CH₄ fluxes from the FLUXNET-CH₄ dataset, was applied in the comparison. This dataset used a random forest model to
upscale ground-based eddy covariance CH₄ flux data and then was forced with globally-gridded predictor data and two
wetland extent products, to predict wetland CH₄ emissions. The predictors included data sources from climate,
170 biometeorological, and soil properties.

2.4 Time series decomposition and statistical analyses

To attribute the time series of global wetland CH₄ emissions to what we consider the dominant drivers of change (i.e.,
temperature, precipitation, and CO₂ concentration), we applied a multiple regression approach (Piao et al., 2013) to estimate
the parameters of global wetland CH₄ sensitivity to climate drivers using the following equation:

$$175 \quad y = \beta CO_2 + \gamma Tmp + \delta Pre + c + \varepsilon \quad (1)$$

where y is the global annual total wetland CH₄ emission of each model from the transient run, or from the observation-based
upscaling dataset UpCH₄, and Tmp , Pre , and CO_2 are the mean annual temperature, total annual precipitation, and mean
atmospheric CO₂ concentration for that year, respectively. γ , δ , β , and c are regression coefficients and ε is the residual error
term. The regression coefficients were calculated using a maximum likelihood estimate. Changes in other meteorological
180 forcings may also influence the estimation of y . These confounding drivers, such as solar radiation and wind speed, although
they are considered to have minor impacts on the variations of eCH₄, were implicitly accounted for in the regression
coefficients.

2.5 Model factorial experiment

To further separate the contribution of different controls on the change in methane emissions (ΔeCH_4) by climate variations
and rising CO₂, we used a subset of four models that conducted factorial experimental simulations by holding each factor
185 constant during part of the transient runs. This subset of the wetland models (i.e., ELM-ECA, LPJ-wsl, SDGVM, and VISIT)
performed a set of factorial simulations to specifically attribute the effect of temperature, precipitation, and rising CO₂
concentration on wetland CH₄ fluxes with the climatology of 2000-2006 for 2007-2020. The simulations were performed by



running the model keeping one-factor constant at a time to estimate the contribution of each component to the total range of
190 variations (Table S2). For these factorial simulations, we evaluated the annual amplitude of wetland eCH₄ as a relative
percentage change to minimize the impacts of different modeling implementation choices, such as different input variables
among models. The effect of the total changes on the relative change in amplitude was represented by the difference between
the transient (one factor is time-varying) and baseline (static at 2000-2006 levels) runs. For simplicity, the relative
contribution of a single driver to eCH₄ variations was quantified as the transient run minus the specific control run. To
195 calculate the contribution of each driver using the subset of the models, we calculated weighting factors per year across the
models, with lower bias resulting in higher weight relative to the full ensemble mean using an inverse function.

2.6 Temperature dependence calculation

To further evaluate the response of eCH₄ to rising temperatures, we calculated the modeled seasonal eCH₄ temperature
dependence, referred to as the apparent Q₁₀ metric at the locations of 34 FLUXNET-CH₄ sites. This seasonal Q₁₀ differs
200 from the intrinsic Q₁₀ prescribed in the parameterization of respiratory processes in each model. Here it represents the overall
response of eCH₄ along geographic temperature gradients. The apparent Q₁₀ is defined as eCH₄ sensitivity to temperature
change. We calculated apparent Q₁₀ based on CH₄ emitting strength over a standard wetland area, which was calculated as
the CH₄ fluxes divided by inundated area on a per-pixel basis to exclude the effect of inundation dynamics. To derive the
temperature sensitivity of eCH₄ at the soil or ecosystem level, we applied the following equation:

$$205 \quad R(i) = R_b(i)Q_{10}^{\frac{T(i) - T_{ref}}{\Gamma}} \quad (2)$$

where R(i) is the net wetland flux at the location of site *i*, R_b(i) is the basal net CH₄ flux at the reference temperature T_{ref}, and
T(i) is ambient temperature. The parameters Q₁₀, $\Gamma = 10^\circ\text{C}$, and T_{ref} = 15°C are all time-independent constants. The Q₁₀
acting on specific time scales can be obtained from eCH₄ at corresponding specific time scales (i.e., seasonal total and annual
total) by fitting an exponential regression with modeled eCH₄ and air temperature from CRU or GSWP3-W5E5. To quantify
210 the uncertainty in observed apparent Q₁₀, we employed 1000 sets of resampled FLUXNET-CH₄ observations generated
based on a Gaussian distribution. The uncertainty range in measured seasonal mean CH₄ fluxes was determined by
aggregating the uncertainty of daily total fluxes obtained through ANN gap filling.

3 Results and Discussion

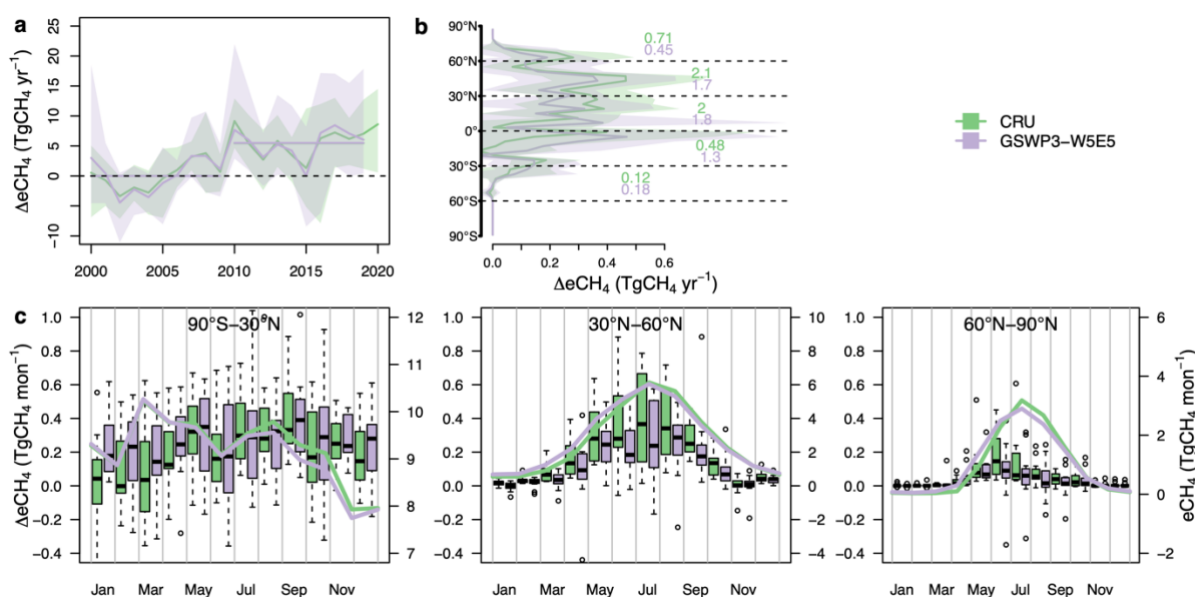
3.1 Changes in eCH₄ during the period of 2000-2020

215 The multi-model ensemble based on the prognostic inundation schemes shows that the average annual global eCH₄ over the
period 2000-2020 was 156±24 Tg CH₄ yr⁻¹ (mean±1σ). The average annual eCH₄ increased from 153 ±23 Tg CH₄ yr⁻¹
during 2000-2009 to 158±24 Tg CH₄ yr⁻¹ during 2010-2020. 15 out of 22 model simulations show significant positive linear
trends (p < 0.01) with an ensemble mean increase rate of 0.6±0.3 Tg CH₄ yr⁻¹ yr⁻¹ over 2000-2020 (Fig. 1a; Table 1; Fig. S2).



Differences in total annual emissions between the two sets of simulations driven by two different climate datasets CRU and
 220 GSWP3-W5E5, agree well in the magnitude of the annual anomalies. Notable eCH₄ variations to climate events were
 observed, such as the rise during the 2010 La Niña (+5.2 Tg CH₄ yr⁻¹) and the decline during the 2015 El Niño (- 4.6 Tg CH₄
 yr⁻¹) after removing the positive linear trends. The multi-model ensemble wetland eCH₄ response to climate events is
 consistent with those reported by earlier studies (Zhang et al., 2018; Zhu et al., 2017) using single wetland models, indicating
 a modulation of the phase of eCH₄ anomaly (ΔeCH_4) by the El Niño-Southern Oscillation. The model ensemble
 225 demonstrates a consistent increase in interannual variability (IAV) in ΔeCH_4 from 3.6 ± 1.6 Tg CH₄ yr⁻¹ during 2000-2009 to
 4.7 ± 1.5 Tg CH₄ yr⁻¹ during 2010-2020, suggesting enhanced wetland-CH₄ sensitivity under climate change.

The models consistently show that 2020 is the strongest positive anomaly year during 2000-2020, with a net increase of 2 [-
 2, 7] Tg CH₄ yr⁻¹ (mean [min, max]) in 2020 compared to 2019. This positive anomaly in 2020 (Table 1) is broadly
 230 consistent with a recent study (Peng et al., 2022) that reported 6 ± 2.3 Tg CH₄ yr⁻¹ based on simulations of two bottom-up
 models with different climate datasets. The discrepancy in estimated magnitude between the Peng et al. (2022) and our
 results is partly due to the parameterizations of wetland area module that causes lower annual magnitude in this study (~
 162 ± 23 Tg CH₄ yr⁻¹ in 2020) compared to the Peng et al. (2022) study (177 ± 31 Tg CH₄ yr⁻¹ in 2020). Additionally, the
 precipitation inputs in the climate forcing used in this study show a lower positive anomaly (~ of 20 mm yr⁻¹ in CRU over
 235 global wetland) in precipitation in 2020 compared to the reanalysis-based estimates (~ 40-117 mm yr⁻¹ over global wetland
 used in the study by Peng et al., (2022)). This discrepancy leads to lower estimates of wetland area and consequently lower
 emissions in this study.





240 **Figure 1: Simulated model ensemble changes of global wetland CH₄ emissions for 2000-2020.** The change is expressed as the
 difference (ΔeCH_4) relative to the mean of the 2000-2009 level from the two sets of simulations with prognostic wetland emission models
 grouped by different climate datasets, CRU and GSWP3-W5E5. a, Time series of annual total anomalies during 2000-2020, with the
 shaded area representing the range between minimum and maximum modeled emissions. The horizontal lines represent the ensemble
 means of 2000-2009 and 2010-2019, respectively. b, Latitudinal gradient of mean ΔeCH_4 , with the mean annual total ΔeCH_4 for each of
 245 the 30° latitude bins from the two sets of simulations shown. c, Boxplots of mean seasonal ΔeCH_4 for the three regions. The central mark
 and the bottom and top edges of the box indicate the median, and the 25th and 75th percentiles of the ensemble, respectively. The colored
 lines represent the average seasonal cycle of 2000-2009 from the simulations grouped by two climate datasets, CRU and GSWP3-W5E5.

There were widespread net increases in eCH_4 across all latitudinal bands during 2010-2020, compared to the average of
 2000-2009, with the largest magnitudes occurring in the 90°S- 30°N bands (there are relatively few wetlands in the southern
 250 extra-tropics 90°S-30°S, contributing 0.1-0.2 Tg CH₄ yr⁻¹) and temperate regions (30-60°N) (Fig. 1b). The annual magnitude
 of eCH_4 increased by 3.7-3.8 Tg CH₄ yr⁻¹, 1.8-2.4 Tg CH₄ yr⁻¹, and 0.6-0.8 Tg CH₄ yr⁻¹ in the tropical, temperate, and Arctic
 wetlands, respectively. The tropics have experienced the largest increases in annual total emissions with an increase of 3%
 relative to 2000-2009 (Table 1). This finding is aligned with the results of several recent atmospheric inversions (Basu et al.,
 2022; Feng et al., 2022; Lan et al., 2021) using satellite observations and/or isotopic measurements that suggest a large
 255 increase in microbial emissions for post-2007 period in the tropics. While the increase in annual total emissions from
 temperate wetlands is lower than that from the tropics, they nevertheless show a larger relative increase of 5-8% compared to
 2000-2009. Arctic wetlands also show an increased rate of 5-7% relative to the same period.

The increase in eCH_4 occurs in parallel with differing patterns of enhanced seasonal cycles between tropical and
 260 extratropical wetlands (30°N-90°N) (Fig. 1c). In temperate and Arctic wetlands, the majority of the increase in emissions
 (60-92%) occurred primarily during the growing season (May-October). Specifically, increases in Arctic wetlands occurred
 during the early growing season (May-July), aligning with findings from a data-driven estimate (Yuan et al., 2024) and a
 long-term eddy covariance-based study (Rößger et al., 2022) that observed early growing season increases in eCH_4 due to
 continuous warming in a Siberian wetland. In contrast, the increase in emissions within the 90°S-30°N band exhibited
 265 relatively minor seasonal variations throughout the year, with the May-October period accounting for a 24% greater increase
 in ΔeCH_4 compared to the November-April period (Fig. S3).

Table 1. Summary of wetland CH₄ emissions (Tg CH₄ yr⁻¹) over different time periods by latitudinal bands for the prognostic wetland simulations. The ensemble mean with minimum and maximum (numbers within brackets) are listed, respectively.

Time period	Forcing	90°S-30°S	30°S-30°N	30°N-60°N	60°N-90°N	Global
2000-2009	CRU	3[1-5]	107[63-141]	31[16-60]	11[4-29]	152[119-187]
	GSWP3-W5E5	3[1-5]	106[60-142]	33[18-57]	11[4-29]	153[116-188]



2010-2019	CRU	3[1-6]	110[67-144]	34[17-64]	12[4-30]	158[126-193]
	GSWP3-W5E5	3[1-6]	110[64-146]	35[18-60]	12[4-29]	158[118-203]

270 3.2 Spatial distribution of eCH₄

A few key regions contribute significantly to global emissions (Fig. 2a,c). These regions are mainly floodplains located along major river basins such as the Amazon, Ganges, Mississippi, and Yangtze; tropical peatlands in the Congo and Southeastern Asia; and high-latitude peatlands in the Hudson Bay Lowland (HBL) and West Siberian Lowland (WSL). However, inter-model variabilities in eCH₄ reveal varying levels of spatial agreement between models, with the largest
 275 discrepancies coming from South America and Africa. South America is one of the largest contributors to the global total eCH₄. Still, the net change in that region shows only a moderate increase, with diverging trends within the Amazon basin during the 2010s (Fig. 2b,d). The uncertain temporal trends are consistent with a long-term, large-scale atmospheric inversion based on airborne campaigns (Basso et al., 2021). South Asia and Africa are among the regions with the largest increases in the tropics, next to North America, but have high uncertainty with a lower level of agreement among the
 280 (Fig. S4). The model ensemble shows that Northwestern South Asia has a significant percentage increase in eCH₄ during 2010-2019 relative to its average levels from 2000-2009, suggesting a possible high sensitivity of eCH₄ to climate change in this region.

The comparison with previous estimates from bottom-up approaches and top-down atmospheric inversions (Table S3)
 285 suggests that the model ensemble mean generally captures well the spatial distribution of annual eCH₄, with a potential underestimation for a few methane hotspots (Fig. S5). The model ensemble means for the Amazon basin, HBL, and WSL show good agreement with atmospheric inversions (Bergamaschi et al., 2013; Pickett-Heaps et al., 2011; Ringeval et al., 2014; Tunnicliffe et al., 2020; Wilson et al., 2016, 2021) and bottom-up modeling estimates (Bansal et al., 2023; Bloom et al., 2017; Bohn et al., 2015), with relatively low uncertainty. The model ensemble highlights WSL and HBL as CH₄ hotspots
 290 in the high latitudes, with good agreements of annual magnitudes with atmospheric inversions and in situ observations (Bohn et al., 2015; Glagolev et al., 2011; Pickett-Heaps et al., 2011), while the models have lower estimates for Alaska compared to the inversions (Chang et al., 2014; Miller et al., 2016). However, for the two hotspots of the Pantanal and Sudd wetlands, the models tended to underestimate the annual eCH₄ compared to a few recent satellite-based estimates (Gerlein-Safdi et al., 2021; Gloor et al., 2021; Lunt et al., 2021; Pandey et al., 2021), with a large uncertainty range of up to two orders of
 295 magnitude across the model ensemble (Fig. S5). In addition to the regions where eCH₄ are being underestimated, recent studies (France et al., 2022; Shaw et al., 2022) based on aircraft measurements suggest that the bottom-up models likely underestimate high eCH₄ fluxes in some little-studied wetlands, such as those in Zambia and Bolivia. The underestimations by process-based wetland models can be attributed to: 1) the challenge in accurately capturing the areal dynamics of



wetlands under varying hydrological conditions, such as in flat terrains that receives lateral transport of water from upper
 300 streams (Li et al., 2024; Lunt et al., 2021; Gerlein-Safdi et al., 2021); 2) existing knowledge gaps in mapping wetlands in
 remote areas, which affect the parameterization of inundation modeling; 3) the limited representation of water table
 regulation (Chen et al., 2021) and wetland PFTs (Bastviken et al., 2023) on eCH₄ in biogeochemical models.

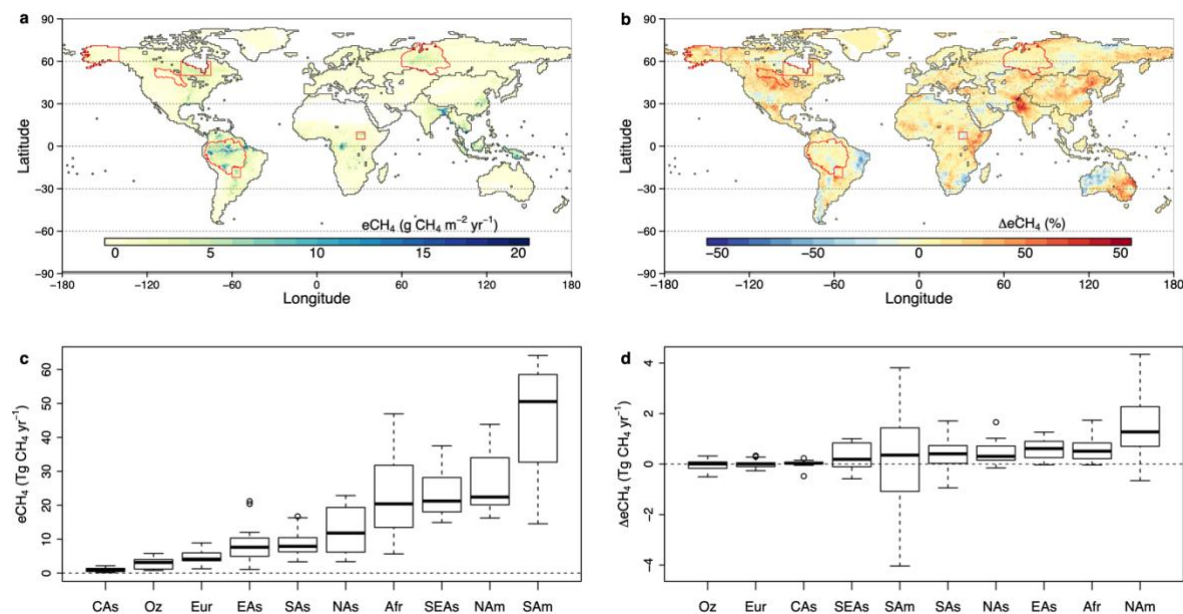


Figure 2. Spatial distribution of eCH₄ and the average change between the 2010s and 2000s. a. Map of mean eCH₄ (Unit: gCH₄ m⁻²
 305 yr⁻¹ per 0.5 deg grid cell) for 2000-2020. The regions defined in c, d and regional CH₄ hotspots in Table S3 are outlined in black and in
 red, respectively. b. Map of change in mean annual wetland emissions (ΔeCH₄) between the 2010s and 2000s. c. Boxplot of mean annual
 eCH₄ and d. ΔeCH₄ by regions for 2000-2020 in ascending order for median estimates, Afr: Africa; CAs: Central Asia; EAs: East Asia;
 Eur: Europe; NAM: North America; NAs: North Asia; Oz: Oceania; SAM: South America; SAs: South Asia; SEAs: Southeast Asia.

310 3.2 Attribution of wetland CH₄ changes

To evaluate the relative contribution of different factors on global eCH₄, we calculated the sensitivity of eCH₄ to mean
 annual temperature (denoted as γ), annual total precipitation (denoted as δ), and CO₂ concentration (denoted as β) using a
 multiple regression approach for each model run over the period of 2000-2020. We also carried out factorial simulations for
 a subset of models. The same approach was applied to the upscaled gridded machine learning dataset UpCH₄, which uses
 315 eddy covariance measurements from FLUXNET-CH₄ as training inputs. The model ensemble suggests that temperature is
 the primary driver of the increase in eCH₄ (Fig. 3a). The regression coefficients for γ indicate that for every 1°C increase in
 global mean temperature over wetlands, there is a mean increase in global eCH₄ of 4.6 Tg CH₄ yr⁻¹ °C⁻¹, with a range of -0.4
 and 9.0 Tg CH₄ yr⁻¹ °C⁻¹ between the 10th and 90th percentiles. This mean temperature sensitivity is slightly higher than the γ



coefficient of 3.2-4.1 Tg CH₄ yr⁻¹ °C⁻¹ estimated for UpCH₄. In contrast, precipitation contributed little to the increase from
320 the prognostic simulations, with a coefficient δ of 0 to 0.3 Tg CH₄ yr⁻¹ mm⁻¹. The coefficient δ was lower at -0.05-0 Tg CH₄
yr⁻¹ mm⁻¹ for UpCH₄, as precipitation was not chosen as a model training predictor through its feature selection, based on
site-level eddy covariance measurements (McNicol et al., 2023). However, precipitation is a more dominant factor at large
scales, especially for tropical floodplains, which contribute the largest proportion of emissions but are poorly represented by
eddy covariance measurements. The model ensemble estimated β remains small, ranging from 0 to 0.3 Tg CH₄ yr⁻¹ ppm⁻¹,
325 while UpCH₄ suggests a β at -0.01 Tg CH₄ yr⁻¹ ppm⁻¹. However, other confounding drivers might influence eCH₄ as well,
such as solar radiation, wind speed, and nitrogen deposition. Thus, the inferred sensitivities are implicitly accounted for in
the regression coefficients despite their relatively small impacts compared to the major drivers.

Generally, the factorial simulations of the four-model subset indicated a consistently positive contribution (three out of four)
330 from rising temperature to Δ eCH₄, with a large variability (s.d.=4.3 Tg CH₄ yr⁻¹) of contributions from precipitation (Fig.
S6). The strength of the CO₂ fertilization effect varied among models and was moderate but positive in all models. Two
models (ELM-ECA and SDGVM) were among the models with higher sensitivity to climate variations while LPJ-wsl and
VISIT were close to the full ensemble mean. ELM-ECA produced a negative temperature effect on eCH₄, likely due to its
modeled nutrient constraints and higher temperature sensitivity for methanotrophic compared to methanogenic processes.
335 Considering the deviation of each model from the full ensemble mean, the weighted mean (Fig. S7) contributions for
temperature, precipitation, and CO₂ concentration from the subset models were 3.2, 1.8, and 1.4 Tg CH₄ yr⁻¹, respectively.
The results from the subset of the models consistently demonstrate that temperature is the primary factor influencing eCH₄.

Overall, the interannual variations of modeled eCH₄ were primarily associated with rising temperature, altered precipitation
340 patterns, and rising atmospheric CO₂ concentrations that stimulated ecosystem productivity through the CO₂ fertilization
effect (Yvon-Durocher et al., 2014). We note that a recent study found strong hysteresis in the seasonal temperature
dependence of observed eCH₄ using the FLUXNET-CH₄ dataset (Chang et al. 2021). Those hysteretic features likely result
in uncertainty in annual temperature sensitivity estimates but would not bias the conclusion of temperature as a dominant
controller of eCH₄ at the decadal time scale. The links between rising temperature and enhanced net CH₄ fluxes are evident
345 (as described below), as the annual global average temperature over wetland areas has significantly ($p < 0.01$) increased by
0.5-0.7 °C from 2000-2020 (Fig. 3b). The modeled interannual variations of wetland extent dynamics reproduced the
response to strong climate events (e.g., positive anomaly during the La Niña phase in 2010/2011 (Boening et al., 2012) and
2020). Both climate-forcing datasets suggest no significant trend in the anomaly of annual mean wetland area globally over
the same period based on the prognostic hydrological simulations (Fig. 3b). Similarly, no significant regional trends in
350 wetland area were found for most of the sub-regions, with the exception of South America, which shows a decrease, and
East Asia, which shows a slight increase (Fig. S8). Considering that the extent of modeled wetland areas is primarily driven
by precipitation, we do not detect a substantial contribution of changes in wetland extent to the long-term increase in eCH₄



over 2000-2020 based on the climate datasets. However, considerable differences in annual and seasonal precipitation estimates between the climate datasets used in this study and those derived from reanalysis or satellite-based products (Zhang et al., 2023a) result in large uncertainties in the estimated trends in wetland extent.

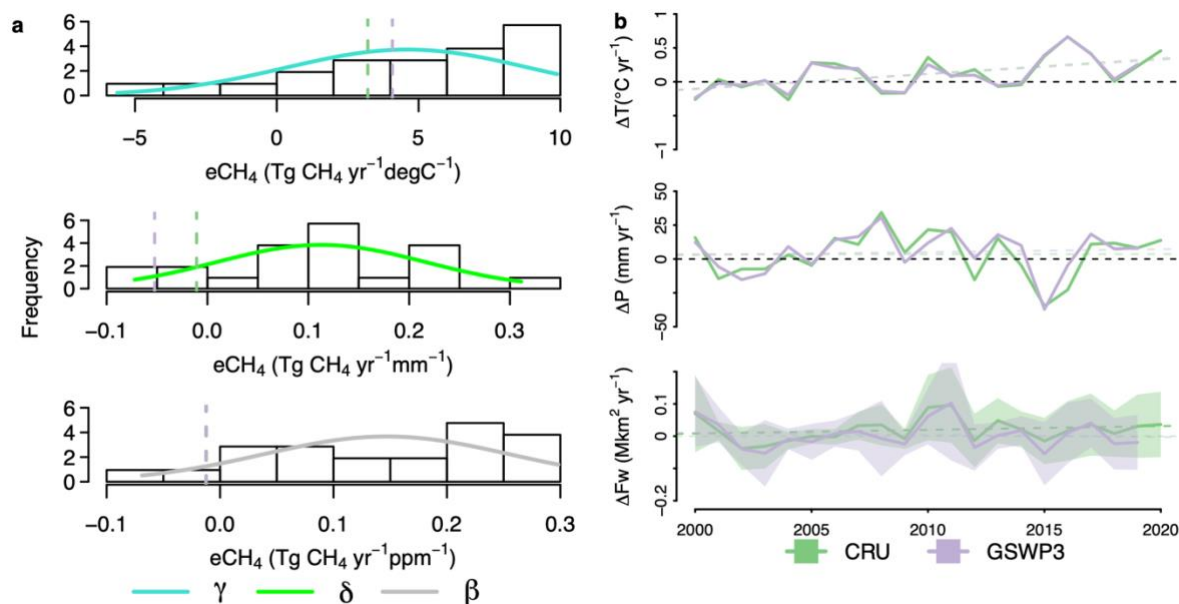


Figure 3. Attributions of $\Delta e\text{CH}_4$ during 2000-2020. a. Histogram showing the sensitivity coefficients derived from a multiple regression approach (See Methods) for temperature (γ), precipitation (δ), and atmospheric CO_2 concentration (β). The curves of density distributions are shown assuming a Gaussian distribution. Vertical lines represent estimates from the machine learning-based dataset UpCH₄, with different colors corresponding to different climate datasets. b. Time series of anomalies for annual mean temperature (ΔT), annual total precipitation (ΔP), and annual mean wetland extent (ΔFw) for 2000-2020 for CRU and 2000-2019 for GSWP3. The shaded area in ΔFw represents the minimum and maximum range from the prognostic model simulations. Dashed lines are linear fitted trends for corresponding variables.

365

3.2 Temperature sensitivity of wetland CH₄ models

The modeled CH₄ emissions show an exponential relationship between eCH₄ and air temperature, with higher temperatures corresponding to higher mean eCH₄ during the peak growing season (JJA, June-July-August) in the Northern Hemisphere (Fig. 4a). The model ensemble mean of eCH₄ response to temperature shows good agreement within the range of the spread when compared to the site-level measurements from FLUXNET-CH₄ and the gridded product UpCH₄. The model ensemble mean has a higher CH₄ emitting strength (i.e., CH₄ emission per standard wetland area) for the high latitudes, leading to lower apparent Q₁₀. This implies that the model ensemble estimated temperature sensitivity for the high latitudes could be

370

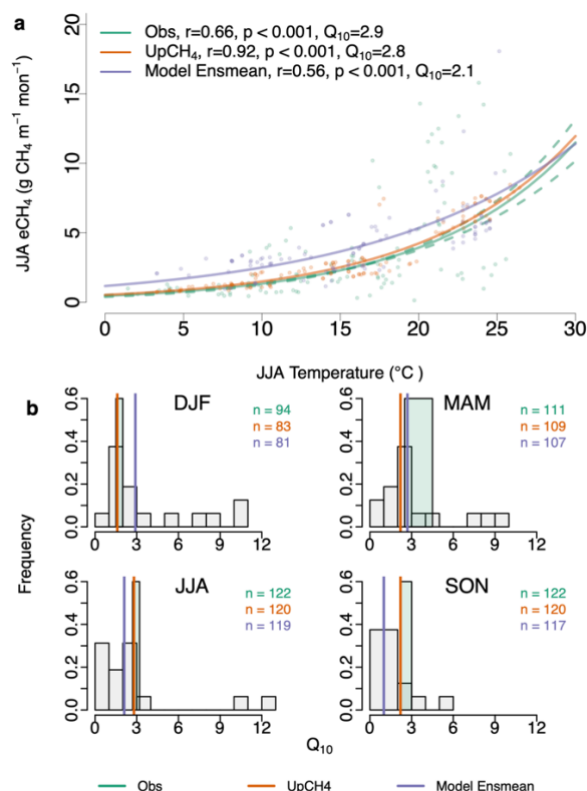


375 potentially overestimated during the JJA season. The apparent Q_{10} values for individual models show a large spread (Fig. S9), with eleven out of the sixteen models having statistically significant ($p < 0.01$) exponential relationships. The good agreement between the ensemble mean and observations suggest that the ensemble approach provides a better constraint compared to single models alone. Furthermore, it is important to acknowledge that the sparse spatial coverage of FLUXNET-CH₄ over low latitudes, especially for underrepresented areas such as Africa, Southeast Asia, and South America, limits our ability to evaluate temperature dependencies over high-temperature regions (Fig. S10).

380 The modeled apparent Q_{10} exhibits an average temperature dependence similar to that of ecosystem respiration, as reported by previous studies (Bloom et al., 2017; Mahecha et al., 2010; Yvon-Durocher et al., 2014), indicating that the underlying factors controlling the response of eCH₄ and ecosystem respiration to temperature covary. The modeled temperature dependences are more constrained with less spread for JJA and SON (September-October-November) than DJF (December-January-February) and MAM (March-April-May) when most site-level measurements have limited availability. The seasonal variations of modeled apparent Q_{10} differ from site-level observations or UpCH₄, reflecting discrepancies in the involved processes between eddy covariance and land surface models. Given that underrepresented processes such as substrate supply tend to have higher sensitivity of ecosystem metabolic processes to temperature, it is likely that the models do not entirely capture the fine-scale processes that affect the overall temperature response (Chang et al. 2021). In addition, the absence or underrepresentation of certain biophysical processes could lead to lower modeled apparent Q_{10} . For instance, the ensemble mean of modeled apparent Q_{10} for SON seasons is underestimated, likely linked to the limited representation of processes during the freeze/thaw cycle (e.g., zero-curtain period), as suggested by previous observational studies (Mastepanov et al., 2008; Zona et al., 2016).

385

390



395 **Figure 4. Temperature sensitivity of simulated seasonal eCH₄ across locations of FLUXNET-CH₄ sites.** a. Model ensemble mean ('Model Ensmean') of simulated eCH₄ against seasonal mean temperature for the JJA season along the temperature gradient at the locations of FLUXNET-CH₄ sites in comparison to the estimates from eddy covariance measurements ('Obs'; Fig. S10; Table S4) and UpCH₄. Each dot represents the value at one site for an individual year when observations are available. The unit of the simulated CH₄ emissions is g CH₄ m⁻¹ month⁻¹ per standard wetland area to exclude the effect of inundation on eCH₄. The exponential fitted curves are shown. b. Histogram of the seasonal Q₁₀ for the 16 individual models for the months DJF, MAM, JJA, and SON. Sample sizes are shown in the plot. The Q₁₀ values derived from FLUXNET-CH₄, UpCH₄, and the model ensemble mean are vertical solid lines, with a width of the bar for 'Obs' indicating the uncertainty range of Q₁₀ based on measurement uncertainty.

400

4 Conclusions

405 Our results estimated global average wetland CH₄ emissions at 158 ± 24 (mean $\pm 1\sigma$) Tg CH₄ yr⁻¹ for the period 2010-2020, with an average decadal increase of 6-7 Tg CH₄ yr⁻¹ compared to the decade of 2000-2009. The increases in the four latitudinal bands of 90°S-30°S, 30°S-30°N, 30°N-60°N, and 60°N-90°N were 0.1-0.2 Tg CH₄ yr⁻¹, 3.6-3.7 Tg CH₄ yr⁻¹, 1.8-2.4 Tg CH₄ yr⁻¹, and 0.6-0.8 Tg CH₄ yr⁻¹, respectively, during the two decades. Our analysis reveals how global wetlands respond to variations in the primary climatic controls of temperature, precipitation, and rising CO₂ concentrations. The



410 model average shows good agreement with eddy covariance measurements on temperature dependence, confirming the
primary role of temperature in the rising trajectory of eCH₄ at decadal timescales. Furthermore, the modeled ensembles of
prognostic wetland extents enable characterization of differences with satellite-based estimates (Prigent et al., 2020; Zhang,
et al., 2021) and their impact on the spatial distribution of global eCH₄. These differences can motivate improvements to
inundation schemes through an improved water table position (Chen et al., 2021) and lateral flow representation. Note that a
415 large portion of tropical wetlands comprises inundated floodplains connecting rivers, where the leaching of methane
production from wetlands to river networks is not accounted for in the wetland models. Resolving the large uncertainty in
wetland areas and seasonal variation remains a high priority to refine bottom-up estimates of eCH₄. Lastly, our results
highlight the important but highly uncertain CO₂ fertilization effect on eCH₄. The factorial experiment results suggest a net
increase of eCH₄ of 0.1%-2.0% relative to the annual total under an average ~20 ppm increase in atmospheric CO₂
420 concentration. In comparison, a synthesis study based on field experiments (van Groenigen et al., 2011) shows a narrower
range of 0.3%-0.6% average increase for every 20 ppm increase, assuming a linear fertilization effect between CO₂
concentration and eCH₄.

Our results show that an ensemble of process-based wetland methane models provides quantification for uncertainty in
425 eCH₄, as well as better constraints than a single model on the predicted trend and magnitude of eCH₄. However, nominally
distinct models might have similar biases because of similarities in the way they represent a subset of processes (see Table
S1 for the model summary). Future evaluation of modeled processes, such as oxidation, production, and transport pathways,
along with model error across different time scales using statistical tools could help identify similarities in model behaviors
to guide model development (Zhang, 2023b). Furthermore, the eCH₄ estimates are subject to forcing uncertainty, given that
430 the two climate datasets applied in the simulation protocol do not cover the full magnitude and variability of climatic
variables. Specifically, precipitation has a significant impact on wetland extent and anaerobic soil conditions but has large
uncertainty in spatiotemporal patterns (Sun et al., 2018). Thus, we recommend future ensemble simulations consider the
uncertainty in climate variables among different datasets. In addition, the sensitivity parameters derived from the multiple
regression are not independent of climate datasets. Thus, they are affected by the choice of meteorological drivers. Overall,
435 quantitatively accounting for model performance and dependence and thoroughly evaluating the effectiveness (Chang et al.,
2023) could improve the wetland model ensemble estimation in future studies.

Code and data availability

The code for the wetland models is available upon request from the respective model groups. The wetland ensemble results
440 is publicly available at the Zenodo Repository 10.5281/zenodo.11309188. The wetland estimates from individual models are
available upon request from respective model groups. The FLUXNET-CH₄ dataset is publicly available at the link:
<https://fluxnet.org/data/fluxnet-ch4-community-product/>. The UpCH₄ dataset can be found at the link in McNicol et al.,
(2023).



445

Author contribution

BP and ZZ designed the simulation experiment with contributions from JM and WR. ZZ conducted data collection and data analysis. JM, WR, GB, PC, NG, PH, AI, AJ, FJ, TK, TL, XL, PM, JM, CP, SP, ZQ, QS, HT, XX, YY, XY, WZ, QZ, QZ, QZ, and ZZ performed the simulations. ZZ prepared the manuscript with contributions from all co-authors.

450

Competing interests

At least one of the (co-)authors is a member of the editorial board of Biogeosciences.

Acknowledgments

455 This paper is the result of a collaborative international effort under the umbrella of the Global Carbon Project, a project of Future Earth, and a research partner of the World Climate Research Programme. Z.Z acknowledge support from National Natural Science Foundation of China Basic Science Center for Tibetan Plateau Earth System project. X. Y and S. Peng were funded by NSFC (41830643, 41722101). Thomas Kleinen acknowledges support from the German Federal Ministry of Education and Research (BMBF), Grant No. 01LP1921A. J.R.M. thanks Jade Skye for her assistance in running and
460 processing the CLASSIC simulations. A. Ito was partly supported by MEXT Arcs-II. L. Liu and Q. Zhuang are supported by NASA project (NNX17AK20G). Q. Zhu and C. Peng are supported by the Second Tibetan Plateau Scientific Expedition (2019QZKK0304). J. Müller and F. Joos were supported by the Swiss National Science Foundation (#200020_200511). Q. Zhu and W. Riley were supported by the Reducing Uncertainties in Biogeochemical Interactions through Synthesis and Computation (RUBISCO) Scientific Focus Area and Energy Exascale Earth System Modeling Project, which are sponsored
465 by the Earth and Environmental Systems Modeling (EESM) Program under the Office of Biological and Environmental Research of the U.S. Department of Energy Office of Science. Y. Yao and H. Tian are funded in part by NSF program (award numbers: # 1903722) NASA CMS Program (award numbers: NX14AO73G). T. Li was supported by the National Key Scientific and Technological Infrastructure project “Earth System Science Numerical Simulator Facility” (EarthLab) and the Open Research Program of the International Research Center of Big Data for Sustainable Development Goals (Grant
470 No. CBAS2023ORP02). P. Hopcroft was supported by a Birmingham Fellowship and the University of Birmingham's BlueBEAR HPC service. W.Z. acknowledges the support from the LUNARC computation project LU 2021/2-114 and the Swedish Research Council (Vetenskapsrådet) starting grant 2020-05338. W.Z. and P.A.M. acknowledge this study as a contribution to the strategic research areas Modeling the Regional and Global Earth System (MERGE) and Biodiversity and Ecosystem Services in a Changing Climate (BECC) at Lund University. RB Jackson acknowledges support from the United
475 Nations Environment Programme (UNEP) to Stanford University DTIE21-EN3143. N.G. was supported by the Newton Fund through the Met Office Climate Science for Service Partnership Brazil (CSSP Brazil). A. Jain and X. Xu were



supported by the US National Science Foundation (NSF- 831361857) and would like to acknowledge the high-performance computing support from Cheyenne (doi:10.5065/D6RX-99HX) provided by NCAR's Computational and Information Systems Laboratory, sponsored by the National Science Foundation. P.C. acknowledges support from the space Agency
480 Climate Change Initiative (ESA CCI) RECCAP2 project (grant no. ESRIN/4000123002/18/I-NB). JG Canadell acknowledges the support of the Australian National Environmental Climate Science Program - Climate Systems hub. G. McNicol acknowledges support from the NASA CMS program (award number: NNH20ZDA001N).

References

- 485 Arndt, K. A., Oechel, W. C., Goodrich, J. P., Bailey, B. A., Kalhori, A., Hashemi, J., Sweeney, C., & Zona, D. (2019). Sensitivity of Methane Emissions to Later Soil Freezing in Arctic Tundra Ecosystems. *Journal of Geophysical Research: Biogeosciences*, *124*(8), 2595–2609. <https://doi.org/10.1029/2019JG005242>
- Arora, V. K., Melton, J. R., & Plummer, D. (2018). An assessment of natural methane fluxes simulated by the CLASS-CTEM model. *Biogeosciences*, *15*(15), 4683–4709. <https://doi.org/10.5194/bg-15-4683-2018>
- 490 Bansal, S., Post van der Burg, M., Fern, R. R., Jones, J. W., Lo, R., McKenna, O. P., Tangen, B. A., Zhang, Z., & Gleason, R. A. (2023). Large increases in methane emissions expected from North America's largest wetland complex. *Science Advances*, *9*(9), eade1112. <https://doi.org/10.1126/sciadv.ade1112>
- Basso, L. S., Marani, L., Gatti, L. V., Miller, J. B., Gloor, M., Melack, J., Cassol, H. L. G., Tejada, G., Domingues, L. G., Arai, E., Sanchez, A. H., Corrêa, S. M., Anderson, L., Aragão, L. E. O. C., Correia, C. S. C., Crispim, S. P., & Neves, R. A.
495 L. (2021). Amazon methane budget derived from multi-year airborne observations highlights regional variations in emissions. *Communications Earth & Environment*, *2*(1), Article 1. <https://doi.org/10.1038/s43247-021-00314-4>
- Bastviken, D., Treat, C. C., Pangala, S. R., Gauci, V., Enrich-Prast, A., Karlson, M., Gålfalk, M., Romano, M. B., & Sawakuchi, H. O. (2023). The importance of plants for methane emission at the ecosystem scale. *Aquatic Botany*, *184*, 103596. <https://doi.org/10.1016/j.aquabot.2022.103596>
- 500 Basu, S., Lan, X., Dlugokencky, E., Michel, S., Schwietzke, S., Miller, J. B., Bruhwiler, L., Oh, Y., Tans, P. P., Apadula, F., Gatti, L. V., Jordan, A., Necki, J., Sasakawa, M., Morimoto, S., Di Iorio, T., Lee, H., Arduini, J., & Manca, G. (2022). Estimating emissions of methane consistent with atmospheric measurements of methane and $\delta^{13}\text{C}$ of methane. *Atmos. Chem. Phys.*, *22*(23), 15351–15377. <https://doi.org/10.5194/acp-22-15351-2022>
- Bergamaschi, P., Houweling, S., Segers, A., Krol, M., Frankenberg, C., Scheepmaker, R. A., Dlugokencky, E., Wofsy, S. C.,
505 Kort, E. A., Sweeney, C., Schuck, T., Brenninkmeijer, C., Chen, H., Beck, V., & Gerbig, C. (2013). Atmospheric CH₄ in the first decade of the 21st century: Inverse modeling analysis using SCIAMACHY satellite retrievals and NOAA surface



- measurements. *Journal of Geophysical Research: Atmospheres*, 118(13), 7350–7369. <https://doi.org/10.1002/jgrd.50480>
- Bloom, A. A., Bowman, K. W., Lee, M., Turner, A. J., Schroeder, R., Worden, J. R., Weidner, R., McDonald, K. C., & Jacob, D. J. (2017). A global wetland methane emissions and uncertainty dataset for atmospheric chemical transport models (WetCHARTs version 1.0). *Geoscientific Model Development*, 10(6), 2141–2156. <https://doi.org/10.5194/gmd-10-2141-2017>
- Boening, C., Willis, J. K., Landerer, F. W., Nerem, R. S., & Fasullo, J. (2012). The 2011 La Niña: So strong, the oceans fell: LA NIÑA 2011-SO STRONG, THE OCEANS FELL. *Geophysical Research Letters*, 39(19), n/a-n/a. <https://doi.org/10.1029/2012GL053055>
- 515 Bohn, T. J., Melton, J. R., Ito, A., Kleinen, T., Spahni, R., Stocker, B. D., Zhang, B., Zhu, X., Schroeder, R., Glagolev, M. V., Maksyutov, S., Brovkin, V., Chen, G., Denisov, S. N., Eliseev, A. V., Gallego-Sala, A., McDonald, K. C., Rawlins, M. A., Riley, W. J., ... Kaplan, J. O. (2015). WETCHIMP-WSL: Intercomparison of wetland methane emissions models over West Siberia. *Biogeosciences*, 12(11), 3321–3349. <https://doi.org/10.5194/bg-12-3321-2015>
- Chang, K.-Y., Riley, W. J., Crill, P. M., Grant, R. F., & Saleska, S. R. (2020). Hysteretic temperature sensitivity of wetland CH₄ fluxes explained by substrate availability and microbial activity. *Biogeosciences*, 17(22), 5849–5860. <https://doi.org/10.5194/bg-17-5849-2020>
- 520 Chang, K.-Y., Riley, W. J., Knox, S. H., Jackson, R. B., McNicol, G., Poulter, B., Aurela, M., Baldocchi, D., Bansal, S., Bohrer, G., Campbell, D. I., Cescatti, A., Chu, H., Delwiche, K. B., Desai, A. R., Euskirchen, E., Friborg, T., Goeckede, M., Helbig, M., ... Zona, D. (2021). Substantial hysteresis in emergent temperature sensitivity of global wetland CH₄ emissions. *Nature Communications*, 12(1), 2266. <https://doi.org/10.1038/s41467-021-22452-1>
- Chang, K.-Y., Riley, W. J., Collier, N., McNicol, G., Fluet-Chouinard, E., Knox, S. H., Delwiche, K. B., Jackson, R. B., Poulter, B., Saunio, M., Chandra, N., Gedney, N., Ishizawa, M., Ito, A., Joos, F., Kleinen, T., Maggi, F., McNorton, J., Melton, J. R., ... Zhuang, Q. (2023). Observational constraints reduce model spread but not uncertainty in global wetland methane emission estimates. *Global Change Biology*, 29, 4298–4312. <https://doi.org/10.1111/gcb.16755>
- 530 Chang, R. Y.-W., Miller, C. E., Dinardo, S. J., Karion, A., Sweeney, C., Daube, B. C., Henderson, J. M., Mountain, M. E., Eluszkiewicz, J., Miller, J. B., Bruhwiler, L. M. P., & Wofsy, S. C. (2014). Methane emissions from Alaska in 2012 from CARVE airborne observations. *Proceedings of the National Academy of Sciences*, 111(47), 16694–16699. <https://doi.org/10.1073/pnas.1412953111>
- 535 Chu, H., Luo, X., Ouyang, Z., Chan, W. S., Dengel, S., Biraud, S. C., Torn, M. S., Metzger, S., Kumar, J., Arain, M. A., Arkebauer, T. J., Baldocchi, D., Bernacchi, C., Billesbach, D., Black, T. A., Blanken, P. D., Bohrer, G., Bracho, R., Brown, S., ... Zona, D. (2021). Representativeness of Eddy-Covariance flux footprints for areas surrounding AmeriFlux sites. *Agricultural and Forest Meteorology*, 301–302, 108350. <https://doi.org/10.1016/j.agrformet.2021.108350>



- Cucchi, M., Weedon, G. P., Amici, A., Bellouin, N., Lange, S., Müller Schmied, H., Hersbach, H., & Buontempo, C. (2020). WFDE5: Bias-adjusted ERA5 reanalysis data for impact studies. *Earth System Science Data*, *12*(3), 2097–2120.
540 <https://doi.org/10.5194/essd-12-2097-2020>
- Delwiche, K. B., Knox, S. H., Malhotra, A., Fluet-Chouinard, E., McNicol, G., Feron, S., Ouyang, Z., Papale, D., Trotta, C., Canfora, E., Cheah, Y.-W., Christianson, D., Alberto, Ma. C. R., Alekseychik, P., Aurela, M., Baldocchi, D., Bansal, S., Billesbach, D. P., Bohrer, G., ... Jackson, R. B. (2021). FLUXNET-CH4: A global, multi-ecosystem dataset and analysis of methane seasonality from freshwater wetlands. *Earth System Science Data*, *13*(7), 3607–3689. <https://doi.org/10.5194/essd-13-3607-2021>
545
- Dirmeyer, P. A., Gao, X., Zhao, M., Guo, Z., Oki, T., & Hanasaki, N. (2006). GSWP-2: Multimodel Analysis and Implications for Our Perception of the Land Surface. *Bulletin of the American Meteorological Society*, *87*(10), 1381–1398. <https://doi.org/10.1175/BAMS-87-10-1381>
- Feng, L., Palmer, P. I., Zhu, S., Parker, R. J., & Liu, Y. (2022). Tropical methane emissions explain large fraction of recent changes in global atmospheric methane growth rate. *Nature Communications*, *13*(1), 1378. <https://doi.org/10.1038/s41467-022-28989-z>
550
- Fleischmann, A. and P., Fabrice and Hamilton, Stephen K. and Fassoni-Andrade, Alice and Wongchuig, Sly and Espinoza, Jhan Carlo and Paiva, Rodrigo and Melack, John and Fluet-Chouinard, Etienne and Castello, Leandro and Almeida, Rafael and Bonnet, Marie Paule and Gripp Alves, Luna and Moreira, Daniel and Yamazaki, Dai and Revel, Menaka and Collischonn, Walter. (2023). Increased floodplain inundation in the Amazon since 1980. *Environmental Research Letters*. <http://iopscience.iop.org/article/10.1088/1748-9326/acb9a7>
555
- Fluet-Chouinard, E., Stocker, B. D., Zhang, Z., Malhotra, A., Melton, J. R., Poulter, B., Kaplan, J. O., Goldewijk, K. K., Siebert, S., Minayeva, T., Hugelius, G., Joosten, H., Barthelmes, A., Prigent, C., Aires, F., Hoyt, A. M., Davidson, N., Finlayson, C. M., Lehner, B., ... McIntyre, P. B. (2023). Extensive global wetland loss over the past three centuries. *Nature*, *614*(7947), 281–286. <https://doi.org/10.1038/s41586-022-05572-6>
560
- France, J. L., Lunt, M. F., Andrade, M., Moreno, I., Ganesan, A. L., Lachlan-Cope, T., Fisher, R. E., Lowry, D., Parker, R. J., Nisbet, E. G., & Jones, A. E. (2022). Very large fluxes of methane measured above Bolivian seasonal wetlands. *Proceedings of the National Academy of Sciences*, *119*(32), e2206345119. <https://doi.org/10.1073/pnas.2206345119>
- Gatti, L. V., Basso, L. S., Miller, J. B., Gloor, M., Gatti Domingues, L., Cassol, H. L. G., Tejada, G., Aragão, L. E. O. C., Nobre, C., Peters, W., Marani, L., Arai, E., Sanches, A. H., Corrêa, S. M., Anderson, L., Von Randow, C., Correia, C. S. C., Crispim, S. P., & Neves, R. A. L. (2021). Amazonia as a carbon source linked to deforestation and climate change. *Nature*, *595*(7867), 388–393. <https://doi.org/10.1038/s41586-021-03629-6>
565
- Gerlein-Safdi, C., Bloom, A. A., Plant, G., Kort, E. A., & Ruf, C. S. (2021). Improving Representation of Tropical Wetland



- Methane Emissions With CYGNSS Inundation Maps. *Global Biogeochemical Cycles*, 35(12), e2020GB006890.
570 <https://doi.org/10.1029/2020GB006890>
- Glagolev, M., Kleptsova, I., Filippov, I., Maksyutov, S., & Machida, T. (2011). Regional methane emission from West Siberia mire landscapes. *Environmental Research Letters*, 6(4), 045214. <https://doi.org/10.1088/1748-9326/6/4/045214>
- Gloor, M., Gatti, L. V., Wilson, C., Parker, R. J., Boesch, H., Popa, E., Chipperfield, M. P., Poulter, B., Zhang, Z., Basso, L., Miller, J., McNorton, J., Jimenez, C., & Prigent, C. (2021). Large Methane Emissions From the Pantanal During Rising
575 Water-Levels Revealed by Regularly Measured Lower Troposphere CH₄ Profiles. *Global Biogeochemical Cycles*, 35(10), e2021GB006964. <https://doi.org/10.1029/2021GB006964>
- Grant, R. F., Mekonnen, Z. A., Riley, W. J., Arora, B., & Torn, M. S. (2017). Mathematical Modelling of Arctic Polygonal Tundra with Ecosys: 2. Microtopography Determines How CO₂ and CH₄ Exchange Responds to Changes in Temperature and Precipitation. *Journal of Geophysical Research: Biogeosciences*, 122(12), 3174–3187.
580 <https://doi.org/10.1002/2017JG004037>
- Harris, I., Jones, P. D., Osborn, T. J., & Lister, D. H. (2014). Updated high-resolution grids of monthly climatic observations - the CRU TS3.10 Dataset: UPDATED HIGH-RESOLUTION GRIDS OF MONTHLY CLIMATIC OBSERVATIONS. *International Journal of Climatology*, 34(3), 623–642. <https://doi.org/10.1002/joc.3711>
- Hopcroft, P. O., Valdes, P. J., O'Connor, F. M., Kaplan, J. O., & Beerling, D. J. (2017). Understanding the glacial methane
585 cycle. *Nature Communications*, 8, 14383. <https://doi.org/10.1038/ncomms14383>
- Kaiser, S., Göckede, M., Castro-Morales, K., Knoblauch, C., Ekici, A., Kleinen, T., Zubrzycki, S., Sachs, T., Wille, C., & Beer, C. (2017). Process-based modelling of the methane balance in periglacial landscapes (JSBACH-methane). *Geoscientific Model Development*, 10(1), 333–358. <https://doi.org/10.5194/gmd-10-333-2017>
- Kirschke, S., Bousquet, P., Ciais, P., Saunois, M., Canadell, J. G., Dlugokencky, E. J., Bergamaschi, P., Bergmann, D.,
590 Blake, D. R., Bruhwiler, L., Cameron-Smith, P., Castaldi, S., Chevallier, F., Feng, L., Fraser, A., Heimann, M., Hodson, E. L., Houweling, S., Josse, B., ... Zeng, G. (2013). Three decades of global methane sources and sinks. *Nature Geoscience*, 6(10), 813–823. <https://doi.org/10.1038/ngeo1955>
- Kleinen, T., Gromov, S., Steil, B., & Brovkin, V. (2023). Atmospheric methane since the last glacial maximum was driven by wetland sources. *Clim. Past*, 19(5), 1081–1099. <https://doi.org/10.5194/cp-19-1081-2023>
- 595 Knox, S. H., Jackson, R. B., Poulter, B., McNicol, G., Fluet-Chouinard, E., Zhang, Z., Hugelius, G., Bousquet, P., Canadell, J. G., Saunois, M., Papale, D., Chu, H., Keenan, T. F., Baldocchi, D., Torn, M. S., Mammarella, I., Trotta, C., Aurela, M., Bohrer, G., ... Zona, D. (2019). FLUXNET-CH₄ Synthesis Activity: Objectives, Observations, and Future Directions. *Bulletin of the American Meteorological Society*, 100(12), 2607–2632. <https://doi.org/10.1175/BAMS-D-18-0268.1>



- 600 Koffi, E. N., Bergamaschi, P., Alkama, R., & Cescatti, A. (2020). An observation-constrained assessment of the climate sensitivity and future trajectories of wetland methane emissions. *Science Advances*, 6(15), eaay4444. <https://doi.org/10.1126/sciadv.aay4444>
- Kuhn, M. A., Varner, R. K., Bastviken, D., Crill, P., MacIntyre, S., Turetsky, M., Walter Anthony, K., McGuire, A. D., & Olefeldt, D. (2021). BAWLD-CH₄: A comprehensive dataset of methane fluxes from boreal and arctic ecosystems. *Earth System Science Data*, 13(11), 5151–5189. <https://doi.org/10.5194/essd-13-5151-2021>
- 605 Li, M., Kort, E. A., Bloom, A. A., Wu, D., Plant, G., Gerlein-Safdi, C., & Pu, T. (2024). Underestimated Dry Season Methane Emissions from Wetlands in the Pantanal. *Environmental Science & Technology*, 58(7), 3278–3287. <https://doi.org/10.1021/acs.est.3c09250>
- Lan, X., Basu, S., Schwietzke, S., Bruhwiler, L. M. P., Dlugokencky, E. J., Michel, S. E., Sherwood, O. A., Tans, P. P., Thoning, K., Etiope, G., Zhuang, Q., Liu, L., Oh, Y., Miller, J. B., Pétron, G., Vaughn, B. H., & Crippa, M. (2021). Improved Constraints on Global Methane Emissions and Sinks Using $\delta^{13}\text{C}$ -CH₄. *Global Biogeochemical Cycles*, 35(6), e2021GB007000. <https://doi.org/10.1029/2021GB007000>
- 610 Lunt, M. F., Palmer, P. I., Lorente, A., Borsdorff, T., Landgraf, J., Parker, R. J., & Boesch, H. (2021). Rain-fed pulses of methane from East Africa during 2018–2019 contributed to atmospheric growth rate. *Environmental Research Letters*, 16(2), 024021. <https://doi.org/10.1088/1748-9326/abd8fa>
- 615 Mahecha, M. D., Reichstein, M., Carvalhais, N., Lasslop, G., Lange, H., Seneviratne, S. I., Vargas, R., Ammann, C., Arain, M. A., Cescatti, A., Janssens, I. A., Migliavacca, M., Montagnani, L., & Richardson, A. D. (2010). Global Convergence in the Temperature Sensitivity of Respiration at Ecosystem Level. *Science*, 329(5993), 838–840. <https://doi.org/10.1126/science.1189587>
- Mastepanov, M., Sigsgaard, C., Dlugokencky, E. J., Houweling, S., Ström, L., Tamstorf, M. P., & Christensen, T. R. (2008). Large tundra methane burst during onset of freezing. *Nature*, 456(7222), 628–630. <https://doi.org/10.1038/nature07464>
- 620 McNicol, G. (2023). Upscaling wetland methane emissions from the FLUXNET-CH₄ eddy covariance network (UpCH₄ v1.0): Model development, network assessment, and budget comparison. *AGU Advances*.
- Meinshausen, M., Vogel, E., Nauels, A., Lorbacher, K., Meinshausen, N., Etheridge, D. M., Fraser, P. J., Montzka, S. A., Rayner, P. J., Trudinger, C. M., Krummel, P. B., Beyerle, U., Canadell, J. G., Daniel, J. S., Enting, I. G., Law, R. M., Lunder, C. R., O'Doherty, S., Prinn, R. G., ... Weiss, R. (2017). Historical greenhouse gas concentrations for climate modelling (CMIP6). *Geoscientific Model Development*, 10(5), 2057–2116. <https://doi.org/10.5194/gmd-10-2057-2017>
- Melton, J. R., Wania, R., Hodson, E. L., Poulter, B., Ringeval, B., Spahni, R., Bohn, T., Avis, C. A., Beerling, D. J., Chen, G., Eliseev, A. V., Denisov, S. N., Hopcroft, P. O., Lettenmaier, D. P., Riley, W. J., Singarayer, J. S., Subin, Z. M., Tian, H., Zürcher, S., ... Kaplan, J. O. (2013). Present state of global wetland extent and wetland methane modelling: Conclusions



- 630 from a model inter-comparison project (WETCHIMP). *Biogeosciences*, 10(2), 753–788. <https://doi.org/10.5194/bg-10-753-2013>
- Miller, S. M., Miller, C. E., Commane, R., Chang, R. Y.-W., Dinardo, S. J., Henderson, J. M., Karion, A., Lindaas, J., Melton, J. R., Miller, J. B., Sweeney, C., Wofsy, S. C., & Michalak, A. M. (2016). A multiyear estimate of methane fluxes in Alaska from CARVE atmospheric observations: METHANE FLUXES FROM ALASKA. *Global Biogeochemical Cycles*, 30(10), 1441–1453. <https://doi.org/10.1002/2016GB005419>
- 635 Natali, S. M., Watts, J. D., Rogers, B. M., Potter, S., Ludwig, S. M., Selbmann, A.-K., Sullivan, P. F., Abbott, B. W., Arndt, K. A., Birch, L., Björkman, M. P., Bloom, A. A., Celis, G., Christensen, T. R., Christiansen, C. T., Commane, R., Cooper, E. J., Crill, P., Czimczik, C., ... Zona, D. (2019). Large loss of CO₂ in winter observed across the northern permafrost region. *Nature Climate Change*, 9(11), 852–857. <https://doi.org/10.1038/s41558-019-0592-8>
- 640 Nisbet, E. G., Manning, M. R., Dlugokencky, E. J., Fisher, R. E., Lowry, D., Michel, S. E., Myhre, C. L., Platt, S. M., Allen, G., Bousquet, P., Brownlow, R., Cain, M., France, J. L., Hermansen, O., Hossaini, R., Jones, A. E., Levin, I., Manning, A. C., Myhre, G., ... White, J. W. C. (2019). Very Strong Atmospheric Methane Growth in the 4 Years 2014–2017: Implications for the Paris Agreement. *Global Biogeochemical Cycles*, 2018GB006009. <https://doi.org/10.1029/2018GB006009>
- 645 Nisbet, E. G., Manning, M. R., Dlugokencky, E. J., Michel, S. E., Lan, X., Röckmann, T., Denier van der Gon, H. A. C., Schmitt, J., Palmer, P. I., Dyonisius, M. N., Oh, Y., Fisher, R. E., Lowry, D., France, J. L., White, J. W. C., Brailsford, G., & Bromley, T. (2023). Atmospheric Methane: Comparison Between Methane’s Record in 2006–2022 and During Glacial Terminations. *Global Biogeochemical Cycles*, 37(8), e2023GB007875. <https://doi.org/10.1029/2023GB007875>
- Palmer, P. I., Woodwark, A. J. P., Finch, D. P., Taylor, T. E., Butz, A., Tamminen, J., Bösch, H., Eldering, A., & Vincent-
650 Bonniou, S. (2022). Role of space station instruments for improving tropical carbon flux estimates using atmospheric data. *Npj Microgravity*, 8(1), 51. <https://doi.org/10.1038/s41526-022-00231-6>
- Pandey, S., Houweling, S., Lorente, A., Borsdorff, T., Tsvilidou, M., Bloom, A. A., Poulter, B., Zhang, Z., & Aben, I. (2021). Using satellite data to identify the methane emission controls of South Sudan’s wetlands. *Biogeosciences*, 18(2), 557–572. <https://doi.org/10.5194/bg-18-557-2021>
- 655 Parker, R. J., Wilson, C., Bloom, A. A., Comyn-Platt, E., Hayman, G., McNorton, J., Boesch, H., & Chipperfield, M. P. (2020). Exploring constraints on a wetland methane emission ensemble (WetCHARTs) using GOSAT observations. *Biogeosciences*, 17(22), 5669–5691. <https://doi.org/10.5194/bg-17-5669-2020>
- Patra, P. K., Houweling, S., Krol, M., Bousquet, P., Belikov, D., Bergmann, D., Bian, H., Cameron-Smith, P., Chipperfield, M. P., Corbin, K., Fortems-Cheiney, A., Fraser, A., Gloor, E., Hess, P., Ito, A., Kawa, S. R., Law, R. M., Loh, Z.,
660 Maksyutov, S., ... Wilson, C. (2011). TransCom model simulations of CH₄ and related species: Linking transport, surface



- flux and chemical loss with CH₄ variability in the troposphere and lower stratosphere. *Atmospheric Chemistry and Physics*, 11(24), 12813–12837. <https://doi.org/10.5194/acp-11-12813-2011>
- Peng, S., Lin, X., Thompson, R. L., Xi, Y., Liu, G., Hauglustaine, D., Lan, X., Poulter, B., Ramonet, M., Saunois, M., Yin, Y., Zhang, Z., Zheng, B., & Ciais, P. (2022). Wetland emission and atmospheric sink changes explain methane growth in 2020. *Nature*, 612(7940), 477–482. <https://doi.org/10.1038/s41586-022-05447-w>
- Piao, S., Sitch, S., Ciais, P., Friedlingstein, P., Peylin, P., Wang, X., Ahlström, A., Anav, A., Canadell, J. G., Cong, N., Huntingford, C., Jung, M., Levis, S., Levy, P. E., Li, J., Lin, X., Lomas, M. R., Lu, M., Luo, Y., ... Zeng, N. (2013). Evaluation of terrestrial carbon cycle models for their response to climate variability and to CO₂ trends. *Global Change Biology*, 19(7), 2117–2132. <https://doi.org/10.1111/gcb.12187>
- 670 Pickett-Heaps, C. A., Jacob, D. J., Wecht, K. J., Kort, E. A., Wofsy, S. C., Diskin, G. S., Worthy, D. E. J., Kaplan, J. O., Bey, I., & Drevet, J. (2011). Magnitude and seasonality of wetland methane emissions from the Hudson Bay Lowlands (Canada). *Atmospheric Chemistry and Physics*, 11(8), 3773–3779. <https://doi.org/10.5194/acp-11-3773-2011>
- Poulter, B., Bousquet, P., Canadell, J. G., Ciais, P., Peregon, A., Saunois, M., Arora, V. K., Beerling, D. J., Brovkin, V., Jones, C. D., Joos, F., Gedney, N., Ito, A., Kleinen, T., Koven, C. D., McDonald, K., Melton, J. R., Peng, C., Peng, S., ... 675 Zhu, Q. (2017). Global wetland contribution to 2000–2012 atmospheric methane growth rate dynamics. *Environmental Research Letters*, 12(9), 094013. <https://doi.org/10.1088/1748-9326/aa8391>
- Prigent, C., Jimenez, C., & Bousquet, P. (2020). Satellite-Derived Global Surface Water Extent and Dynamics Over the Last 25 Years (GIEMS-2). *Journal of Geophysical Research: Atmospheres*, 125(3), e2019JD030711. <https://doi.org/10.1029/2019JD030711>
- 680 Ringeval, B., Houweling, S., van Bodegom, P. M., Spahni, R., van Beek, R., Joos, F., & Röckmann, T. (2014). Methane emissions from floodplains in the Amazon Basin: Challenges in developing a process-based model for global applications. *Biogeosciences*, 11(6), 1519–1558. <https://doi.org/10.5194/bg-11-1519-2014>
- Rößger, N., Sachs, T., Wille, C., Boike, J., & Kutzbach, L. (2022). Seasonal increase of methane emissions linked to warming in Siberian tundra. *Nature Climate Change*, 12(11), 1031–1036. <https://doi.org/10.1038/s41558-022-01512-4>
- 685 Saunois, M., Bousquet, P., Poulter, B., Peregon, A., Ciais, P., Canadell, J. G., Dlugokencky, E. J., Etiope, G., Bastviken, D., Houweling, S., Janssens-Maenhout, G., Tubiello, F. N., Castaldi, S., Jackson, R. B., Alexe, M., Arora, V. K., Beerling, D. J., Bergamaschi, P., Blake, D. R., ... Zhu, Q. (2016). The Global Methane Budget 2000–2012. *Earth System Science Data*, 8(2), 697–751. <https://doi.org/10.5194/essd-8-697-2016>
- Saunois, M., Stavert, A. R., Poulter, B., Bousquet, P., Canadell, J. G., Jackson, R. B., Raymond, P. A., Dlugokencky, E. J., 690 Houweling, S., Patra, P. K., Ciais, P., Arora, V. K., Bastviken, D., Bergamaschi, P., Blake, D. R., Brailsford, G., Bruhwiler, L., Carlson, K. M., Carrol, M., ... Zhuang, Q. (2020). The Global Methane Budget 2000–2017. *Earth System Science Data*,



12(3), 1561–1623. <https://doi.org/10.5194/essd-12-1561-2020>

Schaefer, K., Schwalm, C. R., Williams, C., Arain, M. A., Barr, A., Chen, J. M., Davis, K. J., Dimitrov, D., Hilton, T. W., Hollinger, D. Y., Humphreys, E., Poulter, B., Raczka, B. M., Richardson, A. D., Sahoo, A., Thornton, P., Vargas, R.,
695 Verbeeck, H., Anderson, R., ... Zhou, X. (2012). A model-data comparison of gross primary productivity: Results from the North American Carbon Program site synthesis. *Journal of Geophysical Research: Biogeosciences*, 117(G3).

<https://doi.org/10.1029/2012JG001960>

Schaefer, H., Fletcher, S. E. M., Veidt, C., Lassey, K. R., Brailsford, G. W., Bromley, T. M., Dlugokencky, E. J., Michel, S. E., Miller, J. B., Levin, I., Lowe, D. C., Martin, R. J., Vaughn, B. H., & White, J. W. C. (2016). A 21st-century shift from
700 fossil-fuel to biogenic methane emissions indicated by 13CH₄. *Science*, 352(6281), 80–84.
<https://doi.org/10.1126/science.aad2705>

Shaw, J. T., Allen, G., Barker, P., Pitt, J. R., Pasternak, D., Bauguitte, S. J.-B., Lee, J., Bower, K. N., Daly, M. C., Lunt, M. F., Ganesan, A. L., Vaughan, A. R., Chibesakunda, F., Lambakasa, M., Fisher, R. E., France, J. L., Lowry, D., Palmer, P. I., Metzger, S., ... Nisbet, E. G. (2022). Large Methane Emission Fluxes Observed From Tropical Wetlands in Zambia. *Global
705 Biogeochemical Cycles*, 36(6), e2021GB007261. <https://doi.org/10.1029/2021GB007261>

Shindell, D., & Smith, C. J. (2019). Climate and air-quality benefits of a realistic phase-out of fossil fuels. *Nature*, 573(7774), 408–411. <https://doi.org/10.1038/s41586-019-1554-z>

Shu, S., Jain, A. K., & Kheshgi, H. S. (2020). Investigating Wetland and Nonwetland Soil Methane Emissions and Sinks Across the Contiguous United States Using a Land Surface Model. *Global Biogeochemical Cycles*, 34(7), e2019GB006251.
710 <https://doi.org/10.1029/2019GB006251>

Sun, Q., Miao, C., Duan, Q., Ashouri, H., Sorooshian, S., & Hsu, K.-L. (2018). A Review of Global Precipitation Data Sets: Data Sources, Estimation, and Intercomparisons. *Reviews of Geophysics*, 56(1), 79–107.
<https://doi.org/10.1002/2017RG000574>

Treat, C. C., Bloom, A. A., & Marushchak, M. E. (2018). Nongrowing season methane emissions—a significant component of
715 annual emissions across northern ecosystems. *Global Change Biology*, 24(8), 3331–3343. <https://doi.org/10.1111/gcb.14137>

Tunnicliffe, R. L., Ganesan, A. L., Parker, R. J., Boesch, H., Gedney, N., Poulter, B., Zhang, Z., Lavrič, J. V., Walter, D., Rigby, M., Henne, S., Young, D., & O’Doherty, S. (2020). Quantifying sources of Brazil’s CH₄ emissions between 2010 and 2018 from satellite data. *Atmos. Chem. Phys.*, 20(21), 13041–13067. <https://doi.org/10.5194/acp-20-13041-2020>

van Groenigen, K. J., Osenberg, C. W., & Hungate, B. A. (2011). Increased soil emissions of potent greenhouse gases under
720 increased atmospheric CO₂. *Nature*, 475(7355), 214–216. <https://doi.org/10.1038/nature10176>

Wania, R., Melton, J. R., Hodson, E. L., Poulter, B., Ringeval, B., Spahni, R., Bohn, T., Avis, C. A., Chen, G., Eliseev, A.



- V., Hopcroft, P. O., Riley, W. J., Subin, Z. M., Tian, H., van Bodegom, P. M., Kleinen, T., Yu, Z. C., Singarayer, J. S., Zürcher, S., ... Kaplan, J. O. (2013). Present state of global wetland extent and wetland methane modelling: Methodology of a model inter-comparison project (WETCHIMP). *Geoscientific Model Development*, 6(3), 617–641.
725 <https://doi.org/10.5194/gmd-6-617-2013>
- Wilson, C., Chipperfield, M. P., Gloor, M., Parker, R. J., Boesch, H., McNorton, J., Gatti, L. V., Miller, J. B., Basso, L. S., & Monks, S. A. (2021). Large and increasing methane emissions from eastern Amazonia derived from satellite data, 2010–2018. *Atmospheric Chemistry and Physics*, 21(13), 10643–10669. <https://doi.org/10.5194/acp-21-10643-2021>
- Wilson, C., Gloor, M., Gatti, L. V., Miller, J. B., Monks, S. A., McNorton, J., Bloom, A. A., Basso, L. S., & Chipperfield,
730 M. P. (2016). Contribution of regional sources to atmospheric methane over the Amazon Basin in 2010 and 2011: REGIONAL CH₄ SOURCES IN THE AMAZON BASIN. *Global Biogeochemical Cycles*, 30(3), 400–420. <https://doi.org/10.1002/2015GB005300>
- Xi, Y., Peng, S., Ducharne, A., Ciais, P., Gumbrecht, T., Jimenez, C., Poulter, B., Prigent, C., Qiu, C., Saunois, M., & Zhang, Z. (2022). Gridded maps of wetlands dynamics over mid-low latitudes for 1980–2020 based on TOPMODEL. *Scientific
735 Data*, 9(1), 347. <https://doi.org/10.1038/s41597-022-01460-w>
- Yin, Y., Chevallier, F., Ciais, P., Bousquet, P., Saunois, M., Zheng, B., Worden, J., Bloom, A. A., Parker, R. J., Jacob, D. J., Dlugokencky, E. J., & Frankenberg, C. (2021). Accelerating methane growth rate from 2010 to 2017: Leading contributions from the tropics and East Asia. *Atmospheric Chemistry and Physics*, 21(16), 12631–12647. <https://doi.org/10.5194/acp-21-12631-2021>
- 740 Ying, Q., Poulter, B., Watts, J. D., Arndt, K. A., Virkkala, A.-M., Bruhwiler, L., Oh, Y., Rogers, B. M., Natali, S. M., Sullivan, H., Schiferl, L. D., Elder, C., Peltola, O., Bartsch, A., Armstrong, A., Desai, A. R., Euskirchen, E., Gockede, M., Lehner, B., ... Zhang, Z. (2024). WetCH₄: A Machine Learning-based Upscaling of Methane Fluxes of Northern Wetlands during 2016–2022. *Earth System Science Data Discussions*, 2024, 1–45. <https://doi.org/10.5194/essd-2024-84>
- Yuan, K., Li, F., McNicol, G., Chen, M., Hoyt, A., Knox, S., Riley, W. J., Jackson, R., & Zhu, Q. (2024). Boreal–Arctic
745 wetland methane emissions modulated by warming and vegetation activity. *Nature Climate Change*. <https://doi.org/10.1038/s41558-024-01933-3>
- Yvon-Durocher, G., Allen, A. P., Bastviken, D., Conrad, R., Gudasz, C., St-Pierre, A., Thanh-Duc, N., & del Giorgio, P. A. (2014). Methane fluxes show consistent temperature dependence across microbial to ecosystem scales. *Nature*, 507(7493), 488–491. <https://doi.org/10.1038/nature13164>
- 750 Zhang, Z., Poulter, B., Feldman, A. F., Ying, Q., Ciais, P., Peng, S., & Li, X. (2023a). Recent intensification of wetland methane feedback. *Nature Climate Change*, 13, 430–433. <https://doi.org/10.1038/s41558-023-01629-0>
- Zhang, Z., Bansal, S., Chang, K.-Y., Fluet-Chouinard, E., Delwiche, K., Goeckede, M., Gustafson, A., Knox, S., Leppänen,



- A., Liu, L., Liu, J., Malhotra, A., Markkanen, T., McNicol, G., Melton, J. R., Miller, P. A., Peng, C., Raivonen, M., Riley, W. J., ... Poulter, B. (2023b). Characterizing Performance of Freshwater Wetland Methane Models Across Time Scales at
755 FLUXNET-CH₄ Sites Using Wavelet Analyses. *Journal of Geophysical Research: Biogeosciences*, 128(11), e2022JG007259. <https://doi.org/10.1029/2022JG007259>
- Zhang, Z., Fluet-Chouinard, E., Jensen, K., McDonald, K., Hugelius, G., Gumbrecht, T., Carroll, M., Prigent, C., Bartsch, A., & Poulter, B. (2021). Development of the global dataset of Wetland Area and Dynamics for Methane Modeling (WAD2M). *Earth System Science Data*, 13(5), 2001–2023. <https://doi.org/10.5194/essd-13-2001-2021>
- 760 Zhang, Z., Poulter, B., Knox, S., Stavert, A., McNicol, G., Fluet-Chouinard, E., Feinberg, A., Zhao (赵园红), Y., Bousquet, P., Canadell, J. G., Ganesan, A., Hugelius, G., Hurtt, G., Jackson, R. B., Patra, P. K., Saunio, M., Höglund-Isaksson, L., Huang (黄春林), C., Chatterjee, A., & Li (李新), X. (2021). Anthropogenic emission is the main contributor to the rise of atmospheric methane during 1993–2017. *National Science Review*, nwab200. <https://doi.org/10.1093/nsr/nwab200>
- Zhang, Z., Zimmermann, N. E., Calle, L., Hurtt, G., Chatterjee, A., & Poulter, B. (2018). Enhanced response of global
765 wetland methane emissions to the 2015–2016 El Niño-Southern Oscillation event. *Environmental Research Letters*, 13(7), 074009. <https://doi.org/10.1088/1748-9326/aac939>
- Zhang, Z., Zimmermann, N. E., Stenke, A., Li, X., Hodson, E. L., Zhu, G., Huang, C., & Poulter, B. (2017). Emerging role of wetland methane emissions in driving 21st century climate change. *Proceedings of the National Academy of Sciences*, 114(36), 9647–9652. <https://doi.org/10.1073/pnas.1618765114>
- 770 Zhu, Q., Peng, C., Ciais, P., Jiang, H., Liu, J., Bousquet, P., Li, S., Chang, J., Fang, X., Zhou, X., Chen, H., Liu, S., Lin, G., Gong, P., Wang, M., Wang, H., Xiang, W., & Chen, J. (2017). Interannual variation in methane emissions from tropical wetlands triggered by repeated El Niño Southern Oscillation. *Global Change Biology*, 23(11), 4706–4716. <https://doi.org/10.1111/gcb.13726>
- Zona, D., Gioli, B., Commane, R., Lindaas, J., Wofsy, S. C., Miller, C. E., Dinardo, S. J., Dengel, S., Sweeney, C., Karion, A., Chang, R. Y.-W., Henderson, J. M., Murphy, P. C., Goodrich, J. P., Moreaux, V., Liljedahl, A., Watts, J. D., Kimball, J. S., Lipson, D. A., & Oechel, W. C. (2016). Cold season emissions dominate the Arctic tundra methane budget. *Proceedings of the National Academy of Sciences*, 113(1), 40–45. <https://doi.org/10.1073/pnas.1516017113>